Final report Silicon Photonics Design, Fabrication and Data Analysis

December 1, 2025

Abstract

This report details the complete process of designing an MZI device, encompassing waveguide and MZI simulations, device design and fabrication, and the analysis of experimental data with comparisons to simulation results.

1 Introduction

Currently, silicon photonics is already a mainstream technology in the field of communications, particularly for optical transceivers used in data centers. The major advantage of this technology is that data can be transmitted with lower power consumption while achieving higher data rates. This is possible because different photonic components—such as lasers, modulators, and detectors—can be integrated on a single substrate [1] [2]. The first proposal for a photonic integrated circuit dates back to 1983 [3].

The rapid development in this field has also enabled progress in several other areas, leading to a wide range of applications, such as biomedical sensing [4], LiDAR systems [5], and quantum technologies [6].

The objective of the course project presented in this report is to understand all the steps required to realize a photonic device—from simulation, through design and fabrication, to the measurement of the fabricated devices—while following the design rules and fabrication constraints [7][8].

2 Theory

In this project, a strip waveguide will be modeled and simulated. A detailed discussion of this process is presented in Chapter 3. Based on the simulation results, it is possible to describe a strip waveguide using a compact model. A compact model provides a simpler way to predict the waveguide behavior using experimental data, without explicitly solving Maxwell's equations.

The compact model of a waveguide can be expressed using a Taylor series expansion:

$$n_{\text{eff}}(\lambda) = n_1 + n_2(\lambda - \lambda_0) + n_3(\lambda - \lambda_0)^2 \qquad (1)$$

The Mach-Zehnder Interferometer (MZI) is composed of two beam splitters. To understand its operation, it can be conceptually divided into two stages: a beam splitter and a beam combiner.

The first stage can be represented by a simple Y-branch. The input signal, I_i, is split equally between the two output waveguides, so the intensity of each output waveguide is

$$I_1 = I_2 = \frac{I_i}{2}.$$

The corresponding electric fields in each branch (top and bottom) are

$$E_1 = E_2 = \frac{E_i}{\sqrt{2}}.$$

The second stage is the combiner, where the two waveguides merge into a single output. If both waveguides have the same length and identical propagation properties, the output electric field, E_O, is the sum of the two input fields divided by $\sqrt{2}$:

$$E_O = \frac{E_1 + E_2}{\sqrt{2}}.$$

In the case of a real MZI, each branch may have a different length L, propagation constant β, and propagation loss α. The output intensity is then given by:

$$I_o = \frac{I_i}{4}\left|e^{-i\beta_1 L_1 - \frac{\alpha_1}{2}L_1} + e^{-i\beta_2 L_2 - \frac{\alpha_2}{2}L_2}\right|^2. \quad (2)$$

To simplify this equation, we can assume that the waveguide losses are negligible ($\alpha_1 = \alpha_2 = 0$) and that both branches have identical properties ($\beta_1 = \beta_2 = \beta$). Under these conditions, the output intensity of the MZI simplifies to:

$$I_o = \frac{I_i}{2}\left[1 + \cos(\beta \Delta L)\right]. \quad (3)$$

3 Modelling and Simulation

3.1 Waveguide

In our design, we use a strip waveguide with a width of 500nm and a height of 220nm. We have also taken into account the final profile after the dry etching process. Instead of having an ideal angular profile of 90°, the waveguide exhibits an angular profile of approximately 82°. The simulated waveguide mode profile is shown in Figure 1.

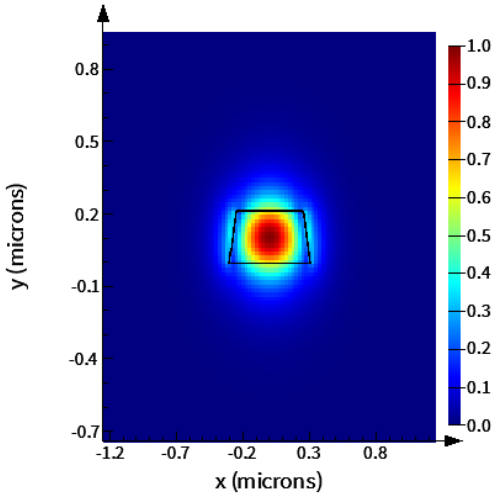

Figure 1: Electric field intensity of TE mode in the waveguide.

From Figure 1, it is observed that nearly all of the light is confined within the waveguide. Furthermore, the fundamental mode is predominantly TE, with approximately 99% of the mode power in the TE polarization. Based on these results, we can estimate the effective index and group index of the waveguide in the TE mode, as shown in Figures 2 and 3.

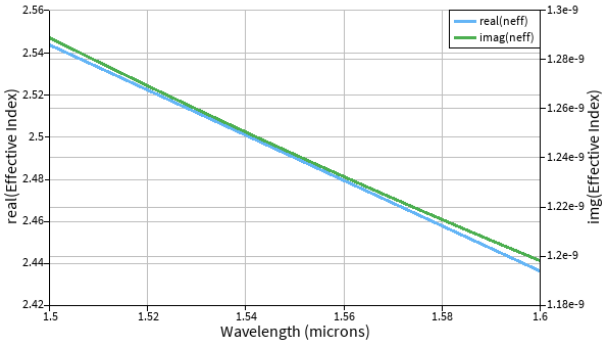

Figure 2: Refractive Index vs wavelength of the simulated waveguide

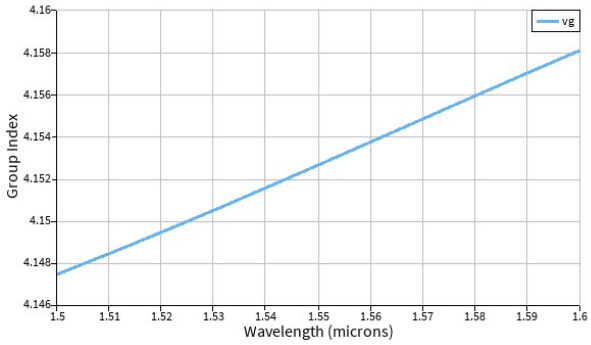

Figure 3: Group Index vs wavelength of the simulated waveguide

As Figures 2 and 3 illustrate, the refractive index decreases with increasing wavelength, while the group index increases with increasing wavelength.

Using a MATLAB script that allows us to simulate the waveguide compact model, we obtained the following expression:

$$n_{\text{eff}}(\lambda) = 2.49 - 1.07(\lambda - \lambda_0) - 0.03(\lambda - \lambda_0)^2 \quad (4)$$

3.2 MZI

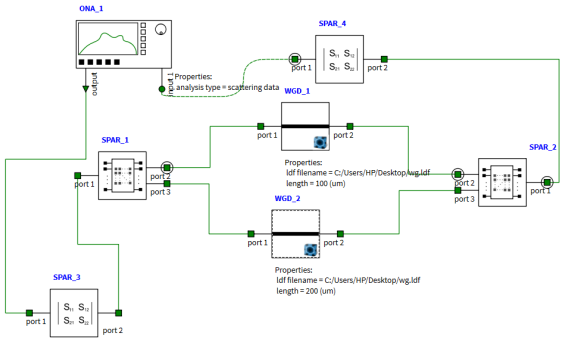

Figure 4: MZI model implemented in the INTERCONNECT software. ONA: optical network analyzer

The MZI device was simulated using the Lumerical Interconnect software. As shown in Figure 4, our model consists of several components. The Y-branches are labeled SPAR1 and SPAR2; the waveguides of different lengths are labeled WGD1 and WGD2; and the grating couplers are labeled SPAR3 and SPAR4. Our simulation model takes into account the losses from both the Y-branches and the grating couplers. The resulting signal from the simulations is presented in Figure 4.

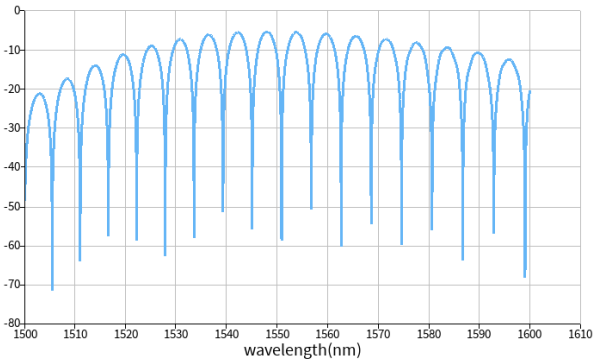

Figure 5: Transfer functions obtained with INTERCONNECT software from a MZI with 100m.

From the simulated signal shown in Figure 5, we can determine that the minimum loss is -5.49dB.

4 Fabrication

The initial design that I proposed for fabrication was as follows:

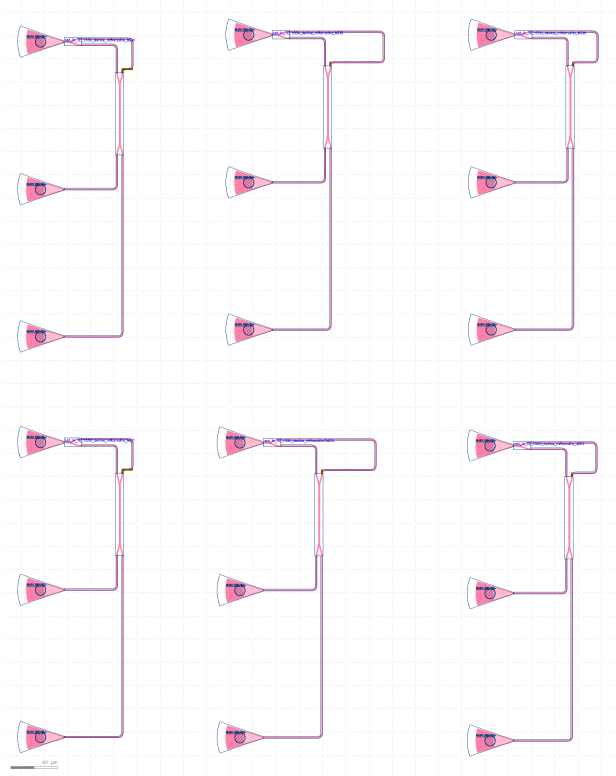

Figure 6: Proposed Klayout design

The original plan was to submit six MZI devices, with three different ΔL values: 25, 50, and 100 m. However, my design did not meet one of the constraints—the available area for printing the devices. I therefore submitted a revised design, in which I removed two devices: one with $\Delta L = 25$ m and another with $\Delta L = 50$ m.

To complete this report, I needed experimental data, which I did not have due to the error I made during the submission process. For this reason, the experimental data analysis was performed using data from three devices provided by another student, whose nickname is RaulNTC. From the several devices he proposed for fabrication, I only used the devices that corresponded to the same MZI configuration with the same ΔL values as in my original design.

After submitting the KLayout design, the devices were sent for fabrication at the Washington Nanofabrication Facility. The schematic in Fig. 12 summarizes all the key steps required to fabricate the devices, from substrate preparation to oxide cladding deposition.

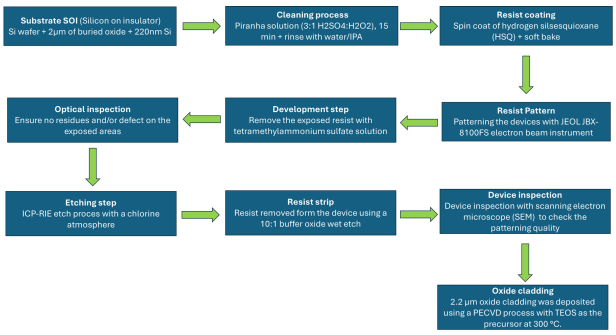

Figure 7: Schematic summarizing all fabrication steps, from substrate preparation to oxide cladding.

When comparing the designed devices with the fabricated ones, there is always some degree of mismatch. These variations may arise either from wafer-to-wafer differences or from variations within the same wafer caused by multiple fabrication steps. Such variations are typically assumed to follow a Gaussian distribution. For wafer-to-wafer variation, the mean value and standard deviation are provided by the supplier. The silicon wafers used in this work have a nominal thickness of 219.6nm, with a 3σ variation of 23.4nm.

Variations within a wafer originate from fabrication processes such as exposure dose fluctuations or etching non-uniformities. As a result, the fabricated waveguide width has an average value of 500nm, with variations of +10nm and –20nm.

To understand the impact of these width and thickness variations on the waveguide, a Cornell analysis was performed by simulating the waveguide while accounting for both types of variation.

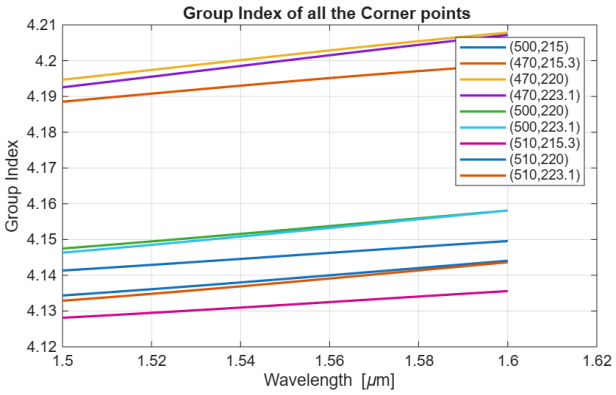

Figure 8: Cornel analysis of the group index in the TE mode.

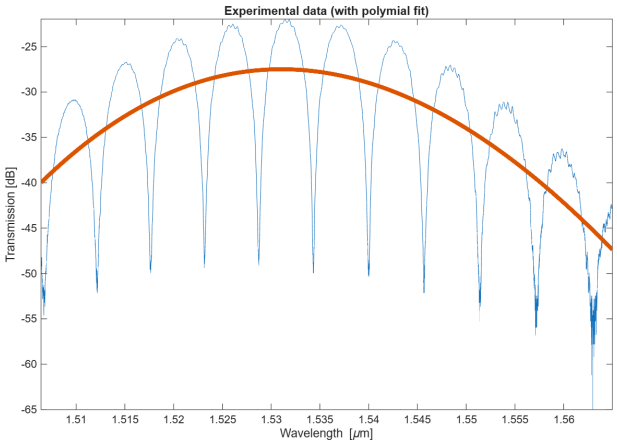

Figure 9: Measurement and baseline correction of the MZI device with ΔL=100m

5 Experimental Data

To characterize the devices, a custom-built automated test setup [[9]] with automated control software written in Python was used (`http://siepic.ubc.ca/probestation`). An Agilent 81600B tunable laser was used as the input source and Agilent 81635A optical power sensors as the output detectors. The wavelength was swept from 1500 to 1600 nm in 10 pm steps. A polarization maintaining (PM) fibre was used to maintain the polarization state of the light, to couple the TE polarization into the grating couplers [[10]]. A 90º rotation was used to inject light into the TM grating couplers [4]. A polarization maintaining fibre array was used to couple light in/out of the chip [www.plcconnections.com]. Plots of experimental data. The following figure was generated using a built-in Python interpreter!

The same experimental procedure was applied to all three devices. For clarity, the procedure will be described only for one device, specifically the one with a length of 100 m. The first observation is that the measured spectrum is not flat but exhibits a curved amplitude response. This behavior arises from the limited bandwidth of the grating coupler.

To remove the baseline introduced by the grating coupler, the data are fitted with a polynomial curve, which is then subtracted from the experimental spectrum. A third-order polynomial was used for this baseline correction.

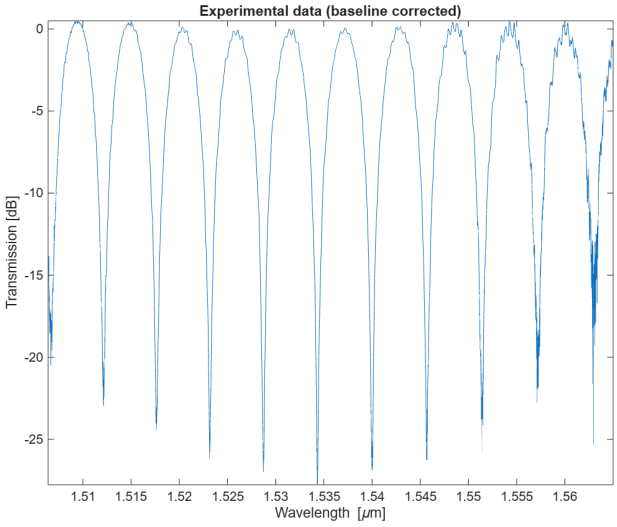

Figure 10: Baseline-Corrected Measurement Data for the MZI with ΔLΔL=100m

After we correct the baseline, we can model the transfer function of an MZI device. The equation that describe the transfer fucntion is the following:

$$F = 10\log\left[\frac{1}{4}\left(1+\exp\left(i\frac{2\pi n_{\text{eff}}}{\Delta L}-\alpha\frac{\Delta L}{2}\right)\right)^2\right]+b \quad (5)$$

where α is the waveguide loss, ΔL is the MZI waveguide length mismatch, b is the excess insertion loss [dB] and n_{eff} is the group reflective index, which is describes by a Taylor expansion, as the equation below shows.

$$n_{\text{eff}}(\lambda\,[\mu\text{m}]) = n_{\text{eff},1} + n_{\text{eff},2}\,(\lambda - 1.55) + n_{\text{eff},3}\,(\lambda - 1.55)^2$$

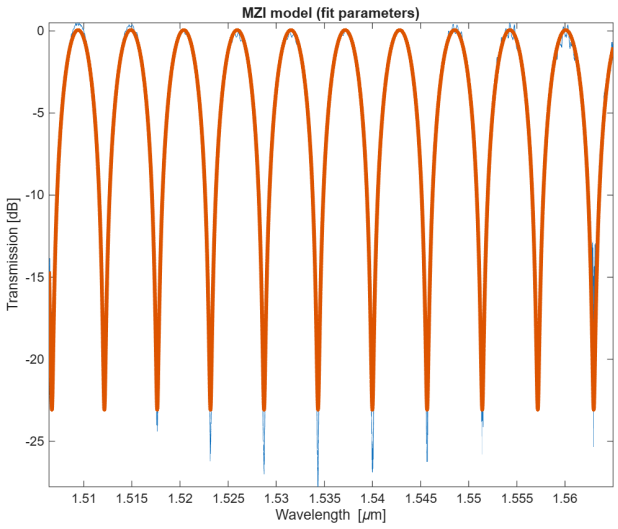

Figure 11: Experimental data of MZI with ΔL=100 , with the fitted model, $n_{\text{eff}} = [2.4457 - 1.1320 - 0.0597]$,$\alpha$ = 0.0028 dB, β = 0.6427 dB

Sample	Experimental n_{eff}	Simulated n_{eff}	Relative Error (%)
MZI 25	4.340	4.152	4.5
MZI 50	4.157	4.153	0.1
MZI 100	4.189	4.153	0.87

Table 1: Comparison between the effective indices (n_{eff}) obtained from experimental measurements and simulations for MZI devices with different path length differences (ΔL). The last column shows the relative percentage error between experimental and simulated values.

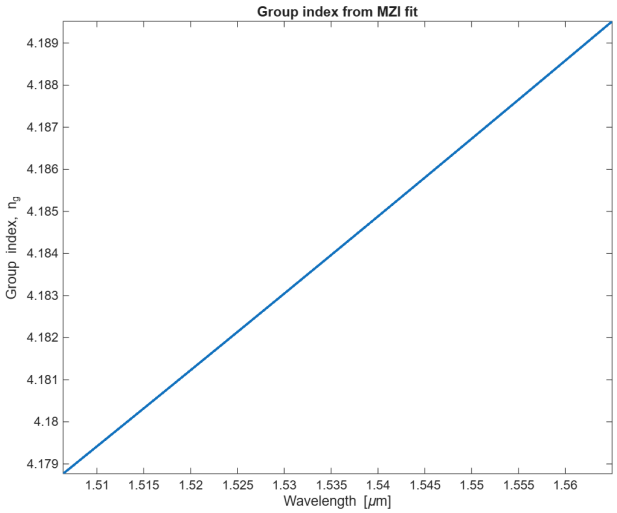

Figure 12: Estimated group index derived from experimental data of a MZI with ΔL=100m

6 Analysis

From the estimated transfer equation of the MZI, it is possible to predict the group index as a function of wavelength for the devices, as shown in Figure 12.

As can be observed, the experimental data follow the same trend as the simulated waveguide data: the group index increases with wavelength. To assess the accuracy of our simulations, we can compare the experimental data with the simulated results and calculate the differences between them, present in Table 1.

7 Conclusion

In this report, we reviewed the entire process of building different MZIs with varying ΔL, starting from simulations, through design and fabrication, and concluding with experimental measurements, which were then compared with the simulated results.

Among the three devices analyzed, two—namely the MZI with $\Delta L = 50$ μm and the MZI with $\Delta L = 100$ μm—showed good agreement with theoretical predictions.

The larger discrepancy observed for the MZI with $\Delta L = 25$ μm can be attributed to its higher sensitivity to small variations during the fabrication process, making it more prone to deviations from the simulated behavior.

8 Acknowledgements

I/We acknowledge the edX UBCx Phot1x Silicon Photonics Design, Fabrication and Data Analysis course, which is supported by the Natural Sciences and Engineering Research Council of Canada (NSERC) Silicon Electronic-Photonic Integrated Circuits (SiEPIC) Program. The devices were fabricated by Richard Bojko at the University of Washington Washington Nanofabrication Facility, part of the National Science Foundation's National Nanotechnology Infrastructure Network (NNIN), and Cameron Horvath at Applied Nanotools, Inc. Enxiao Luan performed the measurements at The University of British Columbia. We acknowledge Lumerical Solutions, Inc., Mathworks, Mentor Graphics, Python, and KLayout for the design software.

References

1. Chrostowski L, Hochberg M (2015) Silicon Photonics Design. Cambridge University Press (CUP)

2. Bojko RJ, Li J, He L, et al. (2011) Electron beam lithography writing strategies for low loss high confinement silicon optical waveguides. Journal of Vacuum Science & Technology B: Microelectronics and Nanometer Structures 29:06F309. https://doi.org/10.1116/1.3653266

1. Manipatruni S, et al. (2018) *Silicon Photonics: The State of the Art*. Wiley-VCH.

2. Bowers JE (2017) *Evolution of Photonic Integrated Circuits*. Optoelectronics Research Group, UCSB.

3. Yariv A, Yeh P (2007) *Optical Waves in Crystals: Propagation and Control of Laser Light*, 5th Edition. Wiley.

4. Lee M, et al. (2024) Photonic Sensors: Current Advancements and Challenges. Sensors 24(3):327. https://doi.org/10.3390/s24030327

5. Hashemi H, et al. (2019) Silicon Photonics for LiDAR: A Review. Applied Sciences 9(20):4225. https://doi.org/10.3390/app9204225

6. Tichy MC, et al. (2021) Integrated Photonics for Quantum Technologies. Quantum Sci Technol 6(2):023002. https://doi.org/10.1088/2058-9565/abe5e1

7. Thomson D, et al. (2023) Roadmapping the Next Generation of Silicon Photonics. arXiv:2305.15820. https://arxiv.org/abs/2305.15820

8. Soref R (2006) The Past, Present, and Future of Silicon Photonics. IEEE J Sel Top Quantum Electron 12(6):1678–1687. https://doi.org/10.1109/JSTQE.2006.884982

9. Chrostowski L, Hochberg M Testing and packaging. In: Silicon Photonics Design. Cambridge University Press (CUP), pp 381–405

10. Wang Y, Wang X, Flueckiger J, et al. (2014) Focusing sub-wavelength grating couplers with low back reflections for rapid prototyping of silicon photonic circuits. Opt Express 22:20652. https://doi.org/10.1364/oe.22.020652